Damage and failure modeling of lotus-type porous material subjected to low-cycle fatigue

J. Kramberger (http://orcid.org/0000-0001-9112-1091)
K. Sterkuš
S. Glodež
University of Maribor, Faculty of Mechanical Engineering
Smetanova 17, SI-2000 Maribor, Slovenia
janez.kramberger@um.si, klemen.sterkus@student.um.si, srecko.glodez@um.si

ABSTRACT. The investigation of low-cycle fatigue behaviour of lotus-type porous material is presented in this paper. Porous materials exhibit some unique features which are useful for a number of various applications. This paper evaluates a numerical approach for determining of damage initiation and evolution of lotus-type porous material with computational simulations, where the considered computational models have different pore topology patterns. The low-cycle fatigue analysis was performed by using a damage evolution law. The damage state was calculated and updated based on the inelastic hysteresis energy for stabilized cycle. Degradation of the elastic stifness was modeled using scalar damage variable. In order to examine crack propagation path finite elements with severe damage were deleted and removed from the mesh during simulation. The direct cyclic analysis capability in Abaqus/Standard was used for low-cycle fatigue analysis to obtain the stabilized response of a model subjected to the periodic loading. The computational results show a qualitative understanding of pores topology influence on low-cycle fatigue under transversal loading conditions in relation to pore orientation.

KEYWORDS. Porous materials; Low-cycle fatigue; Damage; Finite element analysis.

INTRODUCTION

Generally, porous materials are relatively new class of materials with low densities and novel physical, mechanical, thermal, electrical and acoustic properties. These materials present a unique opportunity for adopting in light-weight structures, for energy absorption, for thermal management, and for acoustic absorption [1, 2]. Existing applications are in the mechanical, aerospace and automotive domains [3]. Significant research has been performed regarding optimal manufacturing methods for porous metal material. Current manufacturing methods enable to create various metal foams, either open-celled or closed-celled foams with varying regularity, isotropy and density, perlite metal composites, metallic hollow sphere structures, APM structures etc. [4]. Main factor which affects mechanical properties of porous material is pore structure. For example, porosity of conventional metal foam is high, while mechanical strength is low [5]. On the other hand, lotus-type manufacturing method is capable to produce lotus-type material, which has different pore structure in comparison with metal-foams. The porosity of lotus-type metal is lower and pores are cylindrical and oriented in one direction (Fig. 1). Structural properties of lotus-type porous material depend upon the manufacturing method, cell size and morphology [6].
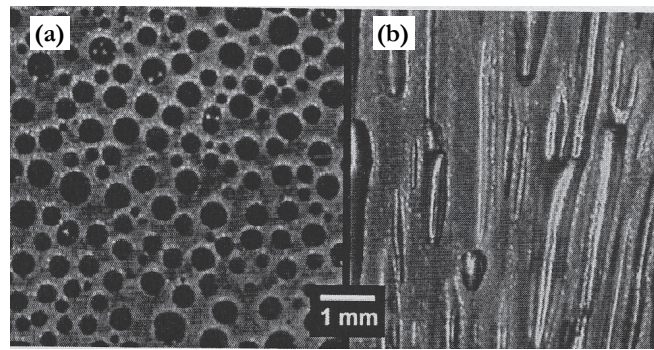
Figure 1: Cross section of lotus-type porous material in transversal (a) and longitudinal (b) direction [6].

Existing research work demonstrates that the most common method for determination of structural properties of porous materials is experimental work [6-9]. Measured mechanical property is usually the compressive yield strength or plateau strength. Other mechanical properties, like elastic modulus, ultimate tensile strength, densification strain and fatigue properties have been less frequently published. In structural applications of porous material, it is necessary to take into account the degradation of strength with cycling loading. However, the fatigue properties of lotus-type porous material have not been clarified in detail, compared with those of metal foams. Seki et al [10] clarified the effect of porosity, anisotropic pore structure, and pore size distribution on the fatigue strength of lotus cooper. They discussed the slip band formation and crack initiation around the pores. Furthermore, fatigue cracks were observed in various cycles of fatigue test, and the crack propagation path was investigated using lotus copper specimens with notch.

This paper discuss the low cycle fatigue behavior of lotus-type porous material and evaluates the fatigue crack initiation and propagation with computational simulations. In this study we used two-dimensional structure as a basis for the finite element analysis. Considered computational models of lotus-type porous material had different pore topology patterns, where both a regular and an irregular pores distribution in transversal direction have been taken into account. The alternate tensile load under displacement rate control was applied and deformation response was examined. Furthermore, damage initiation and evolution were performed using the direct cyclic analysis procedure from Abaqus/Standard to compute the stabilized response of the modeled structure directly in low-cycle fatigue [11, 12].

COMPUTATIONAL METHODS

In recent years computational simulations became an important tool for solving problems in general engineering and science. Computational simulations allow for better insight into analysed structure behaviour and can provide information which is sometimes very difficult or even impossible to determine with experimental measurements. The traditional approach for determining the fatigue limit for a structure is to conduct a transient finite element analysis in which the load cycle is repetitively applied until a stabilized state is obtained [13, 14]. This method can be quite expensive, since it may require application of a large number of loading cycles to obtain the steady response. To overcome this problem, the direct cyclic analysis procedure from Abaqus/Standard was used in this work to compute the stabilized response of the structure directly [11, 12], without having to compute a number of sequential cycles that would lead to such stabilized cycle. Abaqus/Standard offers a general capability for modeling the progressive damage and failure of ductile materials due to stress reversals and the accumulation of inelastic strain energy when the material is subjected to sub-critical cyclic loadings. Damage initiation and evolution criteria are adopted to determine the low-cycle fatigue damage. These two criteria are based on the stabilized accumulated inelastic hysteresis strain energy per cycle, Δw, as illustrated in Fig. 2.

Material failures refer to the complete loss of load-carrying capacity that results from progressive degradation of the material stiffness. The stiffness degradation process is modeled using damage mechanics. The theory of damage mechanics takes into account the process of material degradation due to the initiation, growth and coalescence of micro-cracks/voids in a material element under applied loading. Low-cycle fatigue analysis uses the direct cyclic procedure to directly obtain the stabilized cyclic response of the structure. The direct cyclic procedure combines a Fourier series approximation with time integration of the nonlinear material behavior to obtain the stabilized solution iteratively using modified Newton method. The number of Fourier terms, the number of iterations and the incrementation during the cyclic time period can be controlled to improve accuracy [11].
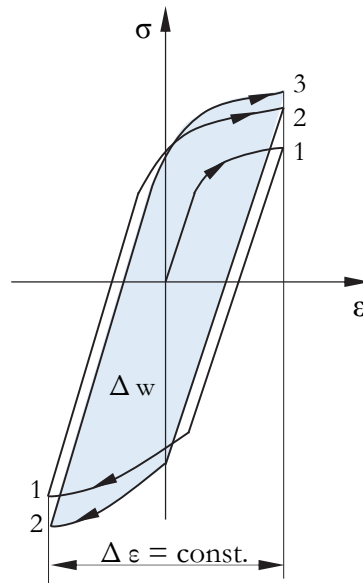
Figure 2: Inelastic hysteresis energy for the stabilized cycle.

The damage initiation criterion is a phenomenological model for predicting the onset of damage due to stress reversals and the accumulation of inelastic strain in a low-cycle fatigue analysis. It is characterized by the accumulated inelastic hysteresis energy per cycle, Δw, in a material point when the structures response is stabilized in the cycle. The cycle number (N_0), in which damage is initiated, is given by:

$$N_0 = c_1 \Delta w^{c_2} \tag{1}$$

where c_1 and c_2 are material constants.

The damage evolution law describes the rate of degradation of the material stiffness per cycle once the corresponding initiation criterion has been reached. For damage in ductile materials Abaqus/Standard assumes that the degradation of the stiffness can be modeled using a scalar damage variable D [11, 15, 16, 17]. At any given cycle during the analysis the stress tensor in the material is given by the scalar damage equation:

$$\sigma = (1 - D)\bar{\sigma} \tag{2}$$

where $\bar{\sigma}$ is the effective (or undamaged) stress tensor that would exist in the material in the absence of damage computed in the current increment. Once the damage criterion is satisfied at the material integration point, the damage state is calculated and updated based on the inelastic hysteresis energy for the stabilized cycle. The rate of damage per cycle is given by:

$$\frac{dD}{dN} = \frac{c_3 \Delta w^{c_4}}{L} \tag{3}$$

where c_3 and c_4 are material constants, and L is the characteristic length associated with the material point and based on the finite element geometry. Material lost its load capacity when $D=1$. When such conditions are satisfied in certain finite element, such element can be removed from the mesh. In such a way damage (crack) propagation can be monitored in computational model.

COMPUTATIONAL MODELS

The discussion from the previous sections shows that the lotus-type porous material behavior is controlled by the porosity. Thus, in this study we have used two-dimensional pore structure as a basis for the finite element simulations. The reasonably homogeneous pore structure of lotus-type porous material was simplified and

represented by the computational models built of multiple representative volume elements (RVEs), as shown in Fig. 3.
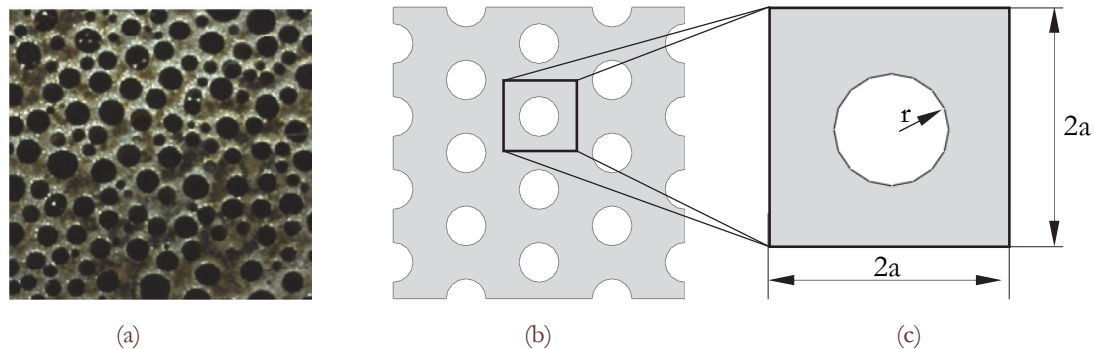

Figure 3: (a) Lotus-type porous iron specimen cross-section [6], (b) geometry of model with shifted pores and (c) geometry of a single RVE with its characteristic parameters: (i) edge length 2a and (ii) pore diameter 2r.

Each RVE is represented by a square block with central cylindrical hole. The length of RVE's edge of 2a = 0.825 mm was determined in the previous study of lotus-type porous material and represents an average RVE size for different porosities of manufactured specimens investigated [6]. Four computational models with different pore topologies presenting lotus-type porous material were studied, as shown in Fig. 4:

a) Regular model with aligned pores: the irregular lotus-type pore distribution was simplified by assuming regular periodic pattern shown in Fig. 4a, where RVEs are aligned in both vertical and horizontal direction.

b) Regular model with 45° rotated aligned pores: this computational model had the same structure as the previous model whereby the aligned pore topology was rotated by 45° around vector parallel to the pore direction, as shown in Fig. 4b.

c) Regular model with shifted pores: the regular model had RVEs stacked in vertical direction with every horizontal line shifted for half of the RVE width of in horizontal direction, as shown in Fig. 4c.

d) Reconstructed irregular model: irregular model was generated by reconstructing the real pore distribution of lotus-type porous specimens, shown in Fig. 4d [6].

The porosity was regulated with change of pore diameter. For first three computational models with regular pore structure, the pore diameter equal 0.55 mm was chosen. The size of each model is a square, 3.3 × 3.3 mm, what corresponded to configuration of 16 RVEs, in model with aligned pores. The porosity of each model was indirectly measured by the use of pre-processing package Abaqus and was equal to 0.234.

The structures, shown in Fig. 4, were used as a basis for FEM analysis of uniaxial loading. The analysis was 2-D under plane strain conditions. Fig. 4 shows the finite element mesh. All models were discretized with plane strain finite elements with linear discretization. The global size of finite elements was chosen equal 0.03 mm, based on parametrical convergence study on simplified model, represented with only one RVE. For model with irregular pores, element size was adjusted to 0.02 in order to satisfy narrow spaces between pores.
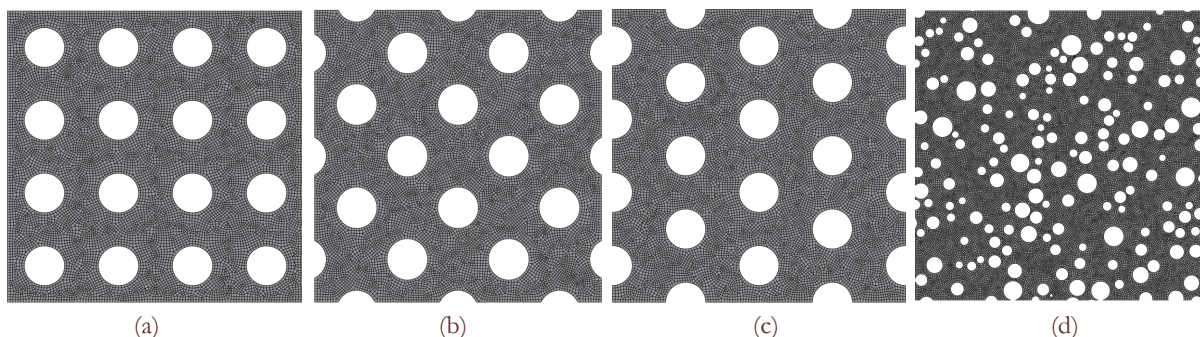

Figure 4: Cross section of lotus-type porous material: (a) aligned, (b) 45° rotated, (c) shifted regular and (d) reconstructed irregular model with porosity of 0.234.

The following isotropic elastic properties were used to describe the behaviour of base material: Young's modulus E = 200 GPa, Poisson's ratio ν = 0.33 and linearized stress–plastic strain relationship given in Tab. 1. The linear kinematic hardening model was used to simulate the cyclic behaviour.

Stress σ [MPa]	Plastic deformation ε_{pl} [-]
400	0
800	24

Table 1: Linearized stress-plastic strain behavior of the base material [11, 16].

The mechanical properties considered in the damage analysis were that of a steel, similar as used in the literature [11, 16, 17]. It is noted that the value c_1 and c_3 is dependent on the system of units in which the model is working.

$c_1 \left(\dfrac{cycle}{N^{c_2}\, mm^{-2c_2}} \right)$	c_2	$c_3 \left(\dfrac{mm}{cycle \left(N^{c_4}\, mm^{-2c_4} \right)} \right)$	c_4
100	-0.6	2.7e-05	1.27

Table 2: Parameters used for damage initiation and evolution prediction [11, 16, 17].

Fig. 5 shows the boundary conditions. On the left and bottom edge symmetric boundary conditions were assumed.
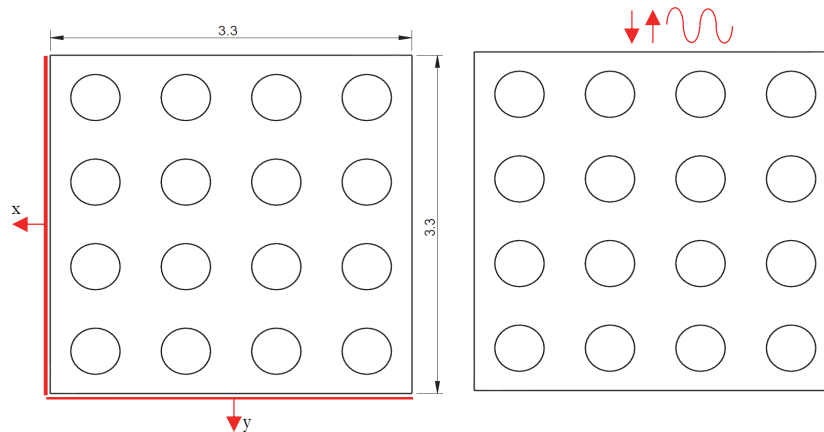

Figure 5: Boundary conditions used for finite element analysis of lotus-type porous material.

The load was applied to the top edge under displacement rate control. Sinusoidal cyclic displacement loading between 0.01 mm and 0.001 mm (load ratio R=0.1) was applied to the low-cycle fatigue steep with a time period of 0.1 seconds. Displacement load at maximum displacement corresponded to the global deformation ε=0.3 %.

COMPUTATIONAL RESULTS AND DISCUSSION

Stress concentrations in computational models at global deformation of 0.3% (elasto-plastic response) are illustrated with equivalent plastic strain PEEQ contours in Fig. 6. The areas with higher plastic strain values denotes locations where material was started to yield first. A large amount of strain localization takes place in the regions around pores.

Fig. 7 shows the evolution of the hysteresis after three loading cycles for global strain range $\Delta\varepsilon$= 0.27%, for all four models. The macroscopic engineering stress σ was determined from the reaction force sum and initial cross-sectional area of the model, while macroscopic engineering strain ε was calculated from the applied displacement and initial length of the

model in the direction of applied load. With increasing cycles, the width of loop increases and the slope decreases. The changes are most predominant for irregular pore structure.
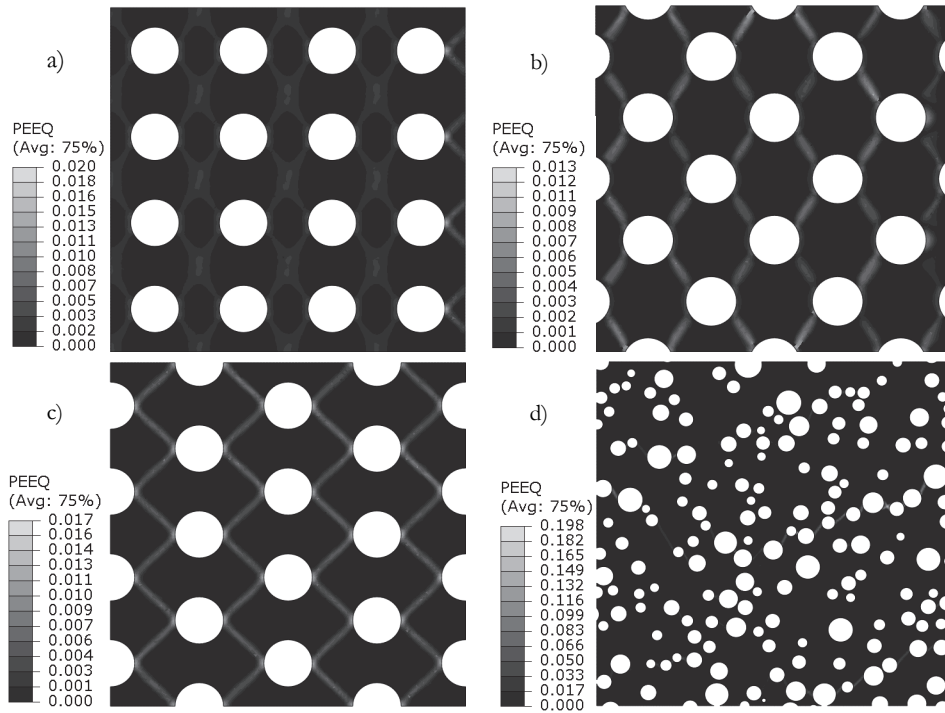

Figure 6: Equivalent plastic strain contours (PEEQ) for global deformation of 0.3% (elasto-plastic response): a) aligned, b) 45° rotated, c) shifted and d) irregular regular models.
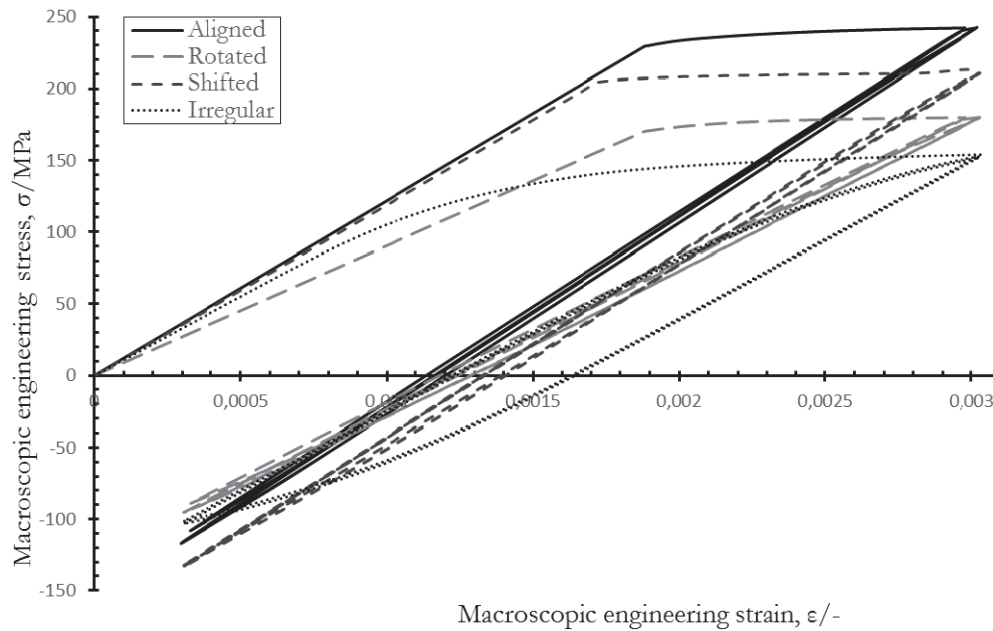

Figure 7: Hysteresis loops observed during 3 fatigue cycles for global strain range $\Delta\epsilon= 0.27\%$.

The damage initiation can be quantified by plotting the number of cycles required to damage initialization (Fig. 8). Strain intensification serves as areas for crack initiation. Our modeling shows that that crack initiation begins the fastest at model with irregular pore structures.
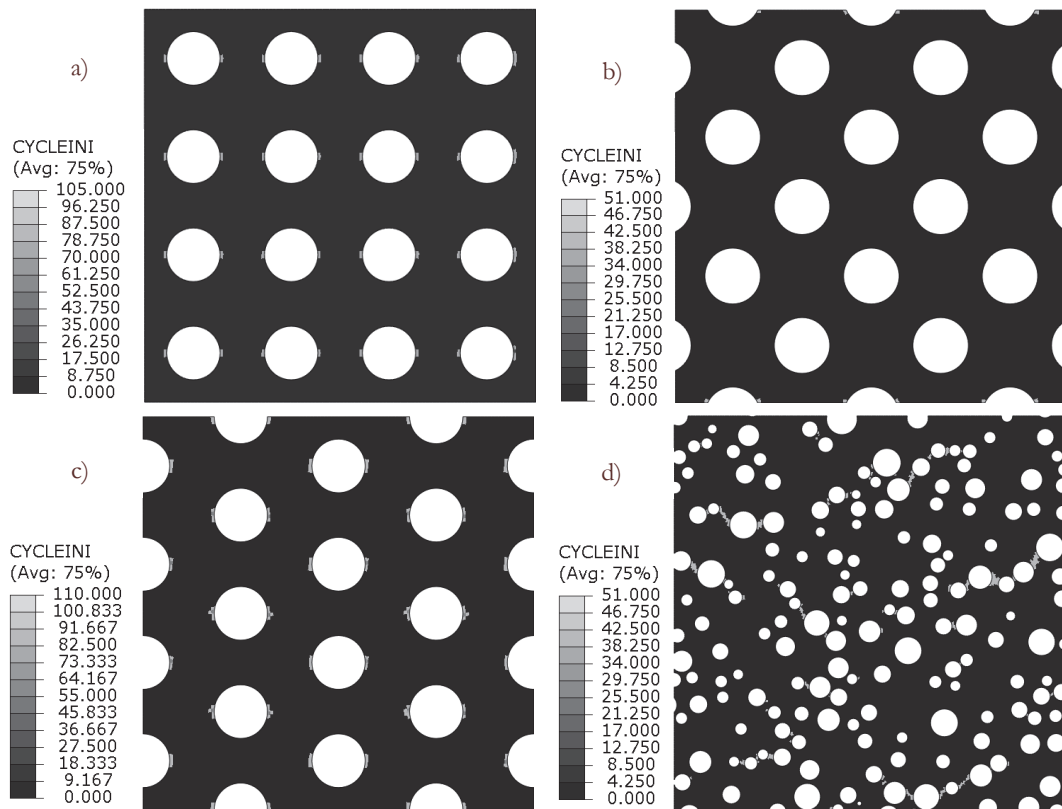
Figure 8: Number of cycles to initialize the damage (CYCLEINI) at the material points for sinusoidal cyclic load: a) aligned, b) 45° rotated, c) shifted and d) irregular pore structure.

Once damage was initiated, the damage parameter D for damage evolution was quantified. In Fig. 9, the contour plot of damage parameter (SDEG) distribution at 100 loading cycles is given. Finite elements, in which damage parameters exceeded value 1.0, were removed from the mesh and are not shown in the Fig. 9. As seen in Fig. 9a, b and c, the damage in regular structures was still localized locally around pores. It is shown in the model with irregular structure (Fig. 9 d) that narrow areas between pores were intensively damaged. The small pores were linked and wider local areas were already cracked. In order to further quantify the damage evolution during fatigue of porous structure, the damage evolution can be monitored.

Figs. 11 through Figs. 13 show damage evolution until approximate prior final fracture. The model with regular aligned (Fig. 10) and irregular (Fig. 13) pore topology demonstrated lower cycle fatigue strength in comparison with the model with regular rotated (Fig. 11) and shifted pores (Fig. 12). Different patterns (crack paths) of damage propagation is also observed. As expected, the cyclic damage evolves gradually, beginning at pore corners and than propagate thru the shortest distance between pores. Porous material exhibits the highest resistance for 45° rotated pore topology (Fig. 11). Some qualitative modeling results of damage evolution was confirmed by experimental worked, available in the literature [7].

CONCLUSIONS

In this study computational modelling was used to study behavior of the lotus-type porous material in low-cycle regime of tensile loading. Numerical simulations have shown the possibility to follow the evolution of damage in lotus-type porous material under fatigue load. Since classical computational approach with simulating the whole load history is computationally intensive, we obtained the stabilized response of the structure subjected to low-cyclic mechanical load using faster direct cyclic algorithm. The efficiency of direct cyclic algorithm was demonstrated on 2-D models. Four types of computational models with simplified regular (aligned, rotated and shifted) and more realistic irregular pore topologies, were considered. It should be noted that the heterogeneous distribution of pores plays a significant role on fatigue behavior of lotus-type material. With the cyclic loading conditions fatigue cracks are formed

around the pores and cracks further propagate between pores in which stress highly concentrates. The computational results show a qualitative understanding of pores topology influence on low-cycle fatigue under transversal tension loading conditions in relation to pore orientation. The results obtained with this study are generally close to those obtained with an experimental approach by other authors [7].

The extension of the approach to more interesting compressive loading conditions of porous material and more complex models will be subject of further research.
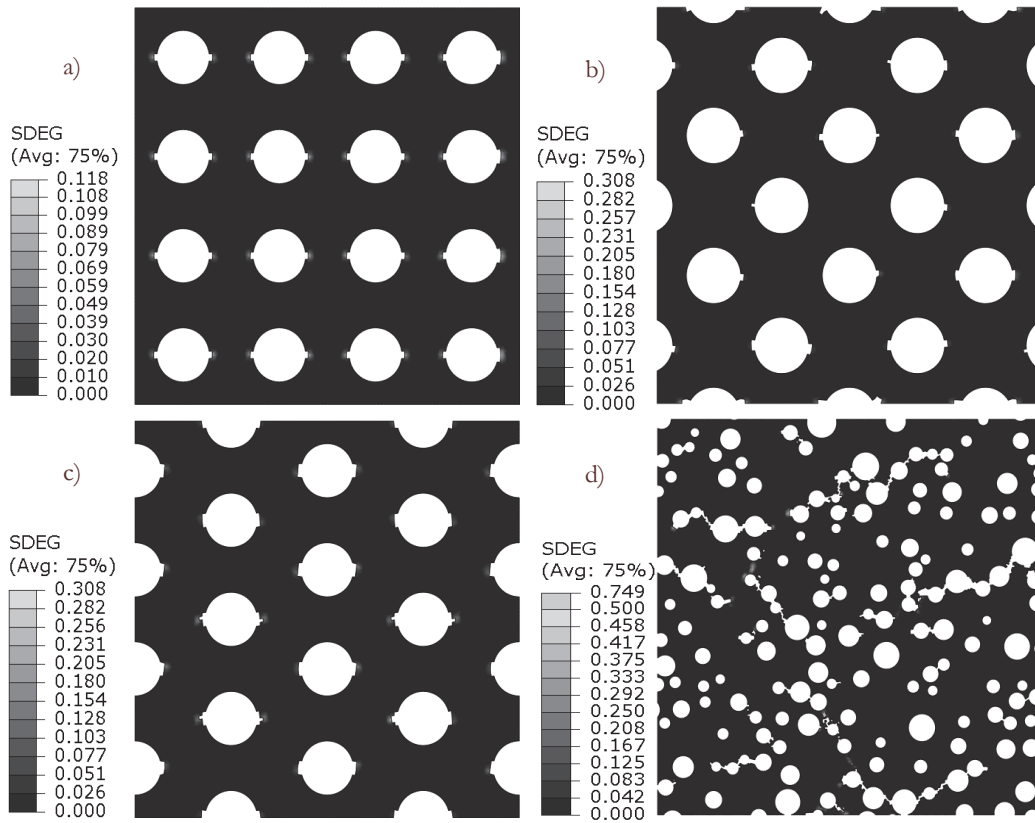

Figure 9: Scalar stiffness degradation (SDEG) (cyclic response after 100 cycles) for: a) aligned, b) 45° rotated, c) shifted and d) irregular pore topology.
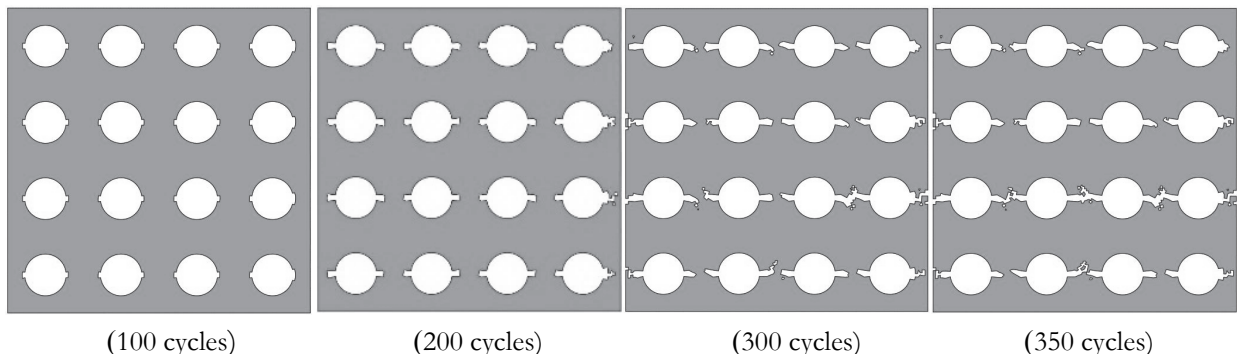

(100 cycles)   (200 cycles)   (300 cycles)   (350 cycles)

Figure 10: Damage evolution in model with regular aligned pore structure.

| (200 cycles) | (300 cycles) | (400 cycles) | (500 cycles) |
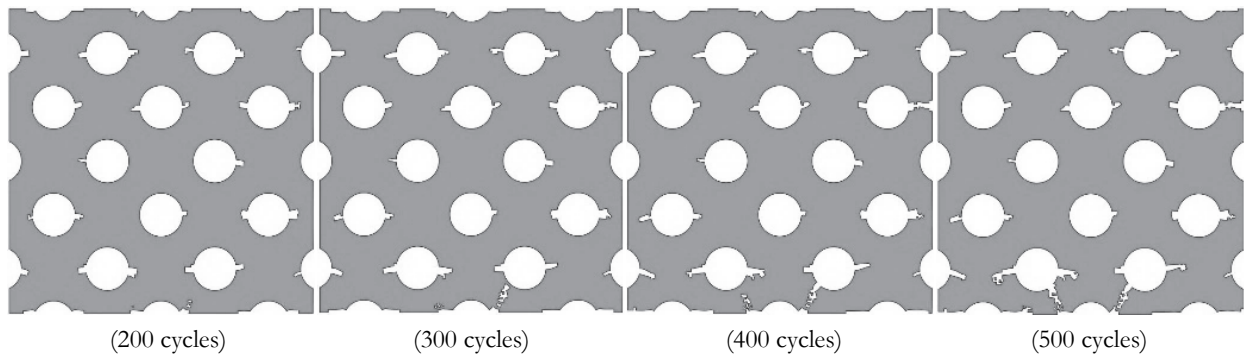
Figure 11: Damage evolution in model with regular 45° rotated pore structure.

| (100 cycles) | (200 cycles) | (300 cycles) | (350 cycles) |
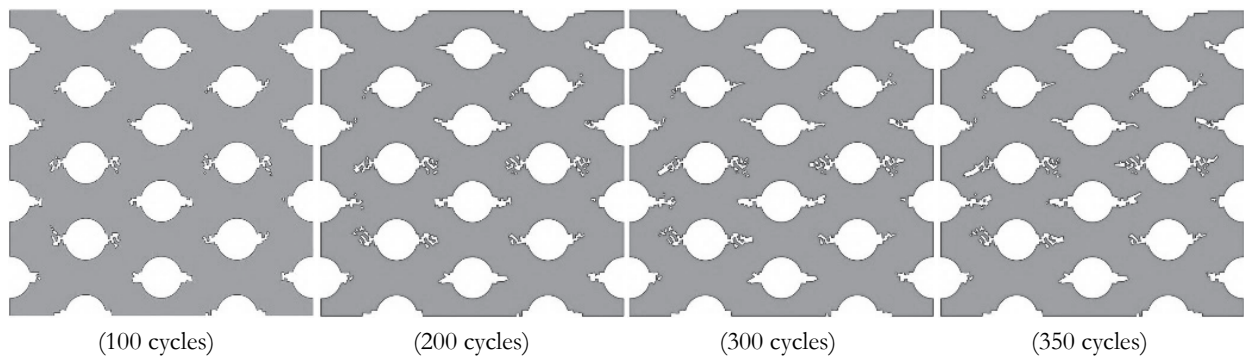
Figure 12: Damage evolution in model with regular shifted pore structure.

| (50 cycles) | (100 cycles) | (150 cycles) | (200 cycles) |
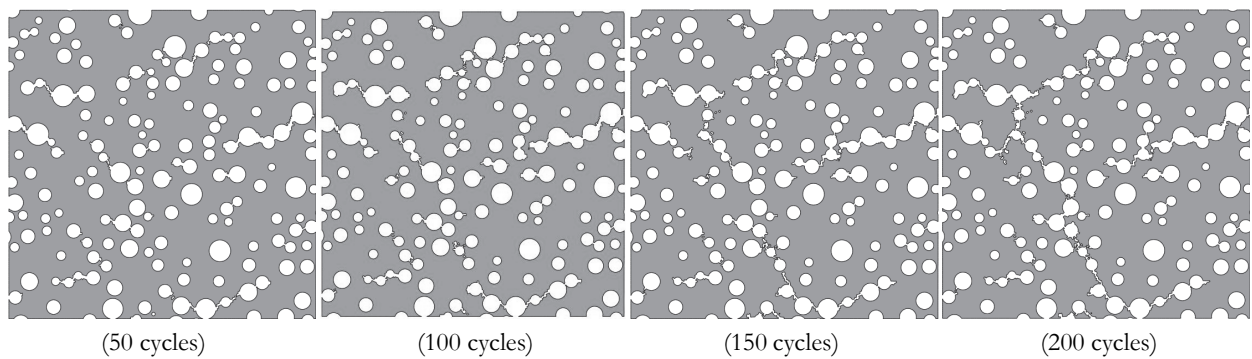
Figure 13: Damage evolution in model with irregular pore structure.

REFERENCES

[1] Ashby, M.F., Tianjian, L.U., Metal foams: A survey, Science in China (Series B), 46 (2003) 521–532.
[2] Gibson, L. J., Ashby, M.F., Cellular Solids: Structure and Properties, Cambridge University Press, Cambridge, (1997).
[3] Smith, B.H., Szyniszewski, S., Hajjar, J.F., Schafer, B.W., Arwade, S.R., Steel foam for structures: A review of applications, manufacturing and Material properties, Journal of Constructional Steel Research 71 (2012) 1–10. DOI: 10.1016/j.jcsr.2011.10.028.

[4] Altenbach, H., Öchsner, A.., (Eds.) Cellular and porous materials in structures and processes, International centre for mechanical sciences, Courses and lectures No. 521(2010), SpringerWienNewYork.

[5] Patrick, J. V., Investigation of the behaviour of open cell aluminium foam, MSc. thesis, University of Massachusetts - Amherst, (2010).

[6] Vesenjak, M., Kovačič, A., Tane, M., Borovinšek, M., Nakajima, H., Ren, Z., Compressive properties of lotus-type porous iron, Comp. Materials Science, 65 (2012) 37–43. DOI: http://dx.doi.org/10.1016/j.commatsci.2012.07.004.

[7] Ide, T., Tane, M., Ikeda, T., Hyun,S.K., Nakajima, H., Compressive properties of lotus-type porous stainless steel, J. Mater. Res., 21 (2006) 185-193. DOI: 10.1557/JMR.2006.0016.

[8] Kramberger, J., Glodež, S., Šraml, M., Porous material: A Review of fatigue behaviour of metal foams, Šolić, S., Šnajdar, M. (Eds.), Proceedings, Croatian society for materials and tribology, (2014) 245-254.

[9] Ingraham, M.D., DeMaria, C.J., Issen, K.A., Morrison, D.J., Low cycle fatigue of aluminum foam, Materials Science and Engineering A 504 (2009) 150–156. DOI: 10.1016/j.msea.2008.10.045.

[10] Seki, H., Tane, M00., Tane, M., Nakajima, H., Fatigue Crack Inititation and Propagation in Lotus-Type Porous Cooper, Comp. Materials Transactions, 49 (2008) 144–150.

[11] Dasault Systemes, SIMULIA, ABAQUS, Online Documentation: Version 6.12.

[12] Nguyen-Tajan, T.M.L., Pommier, B., Maitournam, H., Houari, M., Verger, L., Du, Z.Z, Snyman, M., Determination of the stabilized response of a structure undergoing cyclic thermal-mechanical loads by a direct cyclic method, ABAQUS Users' Conference, (2003).

[13] Chawla, N., Deng,X., Microstructure and mechanical behavior of porous sintered steels, Materials Science and Engineering A 390 (2005) 98–112. DOI: 10.1016/j.msea.2004.08.046.

[14] Andrade Pires, F.M., De Souza Neto, E.A., Owen, D.R.J., On the finite element prediction of damage growth and

[15] fracture initiation in finitely deforming ductile materials, Comput. Methods Appl. Mech. Engrg. 193 (2004) 5223–5256. DOI:10.1016/j.cma.2004.01.038.

[16] Ruzicka, J., Spaniel, M., Prantl, A., Dzugan, J., Kuzelka, J., Moravec, M., Identification of Ductile Damage Parameters in the Abaqus, Bullletin of Applied Mechanics 8 (32) (2012) 89-92.

[17] Pirondi, A., Bonora, N., Modeling ductile damage under fully reversed cycling, Comp. Materials Science, 26 (2003) 129–141.

[18] Čanžar, P., Tonković, Z., Drvar, N., Bakić,A., Kodvanj, J., Sorić, J., Experimental Investigation and Modelling of Fatigue Behaviour of Nodular Cast Iron for Wind Turbine Applications, Proceedings of the 8th International Conference on Structural Dynamics, EURODYN 2011 (2011) 3252-3257.